ELSEVIER

Journal of Nuclear Materials 249 (1997) 58–69

journal of nuclear materials

Determination of the activation energy for the formation of U_3O_8 on UO_2

R.J. McEachern [a,*], J.W. Choi [b], M. Kolář [c], W. Long [a], P. Taylor [a], D.D. Wood [a]

[a] *Research Chemistry Branch, AECL, Whiteshell Laboratories, Pinawa, Manitoba, Canada ROE 1LO*
[b] *R&D Group, Korea Atomic Energy Research Institute, P.O. Box 105, Yusong, Taejon 305-600, South Korea*
[c] *Fuel Waste Technology Branch, AECL, Whiteshell Laboratories, Pinawa, Manitoba, Canada ROE 1LO*

Received 15 January 1997; accepted 27 May 1997

Abstract

Published data for the activation energy of U_3O_8 formation on UO_2 are critically reviewed. The range in reported activation energies is very wide (48–194 kJ mol^{-1}) because of improper deconvolution of the first and second stages of UO_2 oxidation and because of the complex temperature dependence of the reaction kinetics. A general method is then presented for quantitative analysis of nucleation-and-growth kinetics by using X-ray diffraction to measure the rate of product formation on a flat surface. This quantitative method is then used to analyze the kinetic data for the formation of U_3O_8 on the surface of UO_2 disks over the range 168–300°C. The resulting Arrhenius plot is linear, and the activation energy for U_3O_8 formation was found to be 146 ± 10 kJ mol^{-1} (90% confidence interval). The quantitative procedure developed herein can be used to estimate the rate of U_3O_8 formation at low (< 175°C) temperatures, and thus makes an important contribution to the safe dry air storage of used nuclear fuel. © 1997 Elsevier Science B.V.

1. Introduction

It is well known that oxidation of UO_2 is a two-step reaction; the product of the first stage is a tetragonal phase with composition near U_3O_7, whereas that of the second is U_3O_8 [1–3]. The rate of formation of U_3O_8 on nuclear fuel has been studied for over 30 years [2–7], most recently because of the importance of oxidation reactions to dry storage and the ultimate disposal of used nuclear fuel [8–10]. From a practical viewpoint, the production of U_3O_8 is the most important aspect in the air oxidation of UO_2 because the formation of U_3O_8 in a previously defected fuel element can lead to splitting of the sheath [6,11,12]. The resulting release of active U_3O_8 powder into the storage container would then complicate subsequent handling and storage of the fuel.

Although the rate of U_3O_8 formation has been widely studied [1–7,9,10] there remains a significant degree of uncertainty in the estimates of both the rate and activation energy for this process. An accurate assessment of the activation energy for the formation of U_3O_8 is particularly important because the oxidation behavior of used nuclear fuel in dry air storage (at temperatures $\leq$ 175°C) is based on an extrapolation of data obtained at higher temperatures. In the present study we review the results of earlier workers, and then present an improved method of examining the kinetics of U_3O_8 formation on the surface of UO_2 disks, based on measurement of X-ray diffraction (XRD) patterns. An improved estimate of the activation energy for the formation of U_3O_8 was thus derived.

2. Previous studies

Published estimates of the rate of U_3O_8 formation on UO_2 (both unirradiated and used fuel) are summarized in Table 1. The data presented in Table 1 are critically assessed in the following two sections.

* Corresponding author. Tel.: +1-204 753 2311, ext. 2595; fax: +1-204 753 2455.

PII S0022-3115(97)00189-X

2.1. Unirradiated UO_2

Much of the early work [4,13,14] on the formation of U_3O_8 was done by measuring the weight gain throughout the oxidation process, and then fitting the data to a standard model for solid-state reaction kinetics. One equation, which describes the rate of nucleation-and-growth reactions, was developed by Johnson and Mehl [15],

$$f(t) = 1 - \exp\left(\frac{-\pi N_v G^3 t^4}{3}\right), \quad (1)$$

where $f(t)$ is the fraction of the material transformed at time t(s), N_v is the rate of nucleation per unit volume (s^{-1} m^{-3}) and G (m s^{-1}) is the rate of radial growth of the nuclei. The rate of formation, $f(t)$, of U_3O_8 has also been modelled with the Avrami–Erofeev equation [16–18],

$$-\ln[1 - f(t)] = (kt)^m \quad (2)$$

where k (s^{-1}) is a composite rate constant which describes both nucleation and growth, and m is an empirically determined constant.

Aronson et al. [4] oxidized UO_2 powders and fitted their kinetic data to Eq. (1). They estimated the rate of U_3O_8 nucleation, and assumed that the ratio of the rate of nucleation, relative to that of U_3O_8 growth, was constant over the temperature range (278–325°C) studied. Aronson et al. [4] were then able to derive an estimate of 146 kJ mol^{-1} for the activation energy of G, the rate of growth of U_3O_8 nuclei on UO_2 powders.

Walker [13] studied the oxidation of both UO_2 powders and sintered pellets and fitted his weight-gain data to the Johnson–Mehl model (Eq. (1)). He claimed that the shape of the reaction curve could be used to estimate the rate of U_3O_8 nucleation. Moreover, he stated that the rate of nucleation is constant over the temperature range (312–352°C and 279–361°C for powders and pellets respectively) studied. The kinetic data gave values of the activation energy for the growth of U_3O_8 of 134.7 kJ mol^{-1} for powders and 110.5 kJ mol^{-1} for pellets.

Saito [14] oxidized UO_2 powders in the range 315–360°C and reported that the oxidation process could be fitted to Eq. (2) with $m = 3$. He thus obtained an activation energy of 127.6 kJ mol^{-1} for the formation of U_3O_8.

All the above studies were based on the fitting of kinetic data to a standard reaction model and the use of assumptions on the rate of U_3O_8 nucleation. To derive an activation energy for U_3O_8 growth, Walker [13] assumed that the rate of nucleation was independent of temperature. In contrast, Aronson et al. [4] and Saito [14] implicitly assumed that the rate of nucleation and growth have the same temperature dependence; they thus calculated activation energies that represent a composite for both the nucleation and the growth of U_3O_8. The assumptions on the rate of U_3O_8 nucleation that were used in the early

Table 1
Published estimates of the activation energy for the formation of U_3O_8 on UO_2 and used fuel

E_{act} (kJ mol^{-1})	Sample	Temp. range (°C)	Method	Ref.
146	UO_2 powder	278–325	gravimetric	[4]
127.6	UO_2 powder	315–360	gravimetric	[14]
~ 100 [a]	UO_2 microspheres	300–450	gravimetric	[3]
161.5	UO_2 powder	365–400	DTA	[28]
134.7	UO_2 powder	312–352	gravimetric	[13]
110.5	UO_2 pellets	279–361	gravimetric	[13]
170.2	AGR pellet fragments	200–300	gravimetric	[22]
48	AGR pellet fragments	300–550	gravimetric	[22]
124–139	CANDU pellets	200–300	XRD	[7]
102 [b]	LWR pellets	200–250	gravimetric	[24]
163	UO_2 powder	200–350	gravimetric	[6]
170	CANDU pellets	330–350	gravimetric	[6]
67	CANDU pellets	350–450	gravimetric	[6]
172	CANDU fuel element	250–300	progression of oxidation front	[6]
63	CANDU fuel element	300–350	progression of oxidation front	[6]
143	UO_2 pellet fragments	250–350	gravimetric	[25]
109	UO_2 pellet fragments	350–400	gravimetric	[25]
94.5	used LWR fuel	300–400	gravimetric	[25]
140	unirradiated CANDU fragments	175–400	gravimetric	[31]
120	used CANDU fragments	175–400	gravimetric	[31]
194	used LWR fragments	250–360	visual exam.	[32]

[a] The activation energy was observed to vary as a function of oxygen pressure.
[b] The value of 120 kJ mol^{-1} corresponds to the oxidation prior to powder formation. The post-spallation period displayed an activation energy of 160 kJ mol^{-1}.

studies [4,13,14] were not clearly justified. Moreover, the oxidation of UO_2 is in general a two-stage process [1,4] [1],

$$UO_2 \rightarrow U_3O_7/U_4O_9^a \rightarrow U_3O_8 \quad (3)$$

and it is difficult to ascertain the extent to which the formation of the intermediate U_3O_7 interferes with weight-gain data on the rate of U_3O_8 formation.

Boase and Vandergraaf, studying unirradiated UO_2 pellets, found that the relative rates of nucleation and growth are not constant over the temperature range of their experiments (320–460°C) and they thus recognized that their calculated activation energy of 96 kJ mol^{-1} is of questionable validity [6]. Therefore, rather than using the Johnson and Mehl model [15] and making assumptions about the rate of nucleation, they plotted the time for 5, 10 and 50% conversion to U_3O_8, and calculated 'pseudo-activation energies'. An Arrhenius plot of the time required to reach 5, 10 and 50% conversion to U_3O_8 displayed similar behavior for each percent transformed with two distinct regions in the Arrhenius plot. In the range 330–350°C the pseudo-activation energy was 170 kJ mol^{-1} whereas it was 67 kJ mol^{-1} in the range 350–450°C. Tests on unirradiated powders gave a similar Arrhenius plot with two linear regions; the calculated pseudo-activation energy based on the time-to-50% reaction was 163 kJ mol^{-1} in the region 200–350°C. Measurements [6] of the rate of progression of the oxidation front into a defected, unirradiated, element gave qualitatively similar results and activation energies of 172 kJ mol^{-1} at 250–300°C and 62.8 kJ mol^{-1} at 300–350°C.

Boase and Vandergraaf [6] reported their results as 'pseudo-activation energies' because the time required to reach a given percent conversion to U_3O_8 is not necessarily (inversely) proportional to the rate of reaction. Specifically, approximation of the reaction rate with the inverse of the time required to reach a given percent reaction will introduce an error if the reaction kinetics are not linear with time. If there is a significant induction time for the reaction, as is often observed with U_3O_8 formation [1], then the pseudo-activation energies reported by Boase and Vandergraaf will differ from the actual activation energy for U_3O_8 formation. However, the data reported by Boase and Vandergraaf are of immense practical importance, and their use of two activation energies (over different temperature ranges) has proven correct. It has now been clearly shown [21–23] that there are at least two different activation energies (at different temperature ranges) for the formation of U_3O_8, with a change in oxidation behavior around 300–350°C. Thus the results of Aronson et al. [4] and Walker [13] are likely an average activation energy for the two different mechanisms.

White et al. [24] measured the rate of weight gain per unit surface area for LWR pellets oxidized in air between 200 and 250°C. He reported that the kinetic behavior before the initiation of U_3O_8 spallation was different than that observed once U_3O_8 powder formation had begun. The activation energy was found to be 102 kJ mol^{-1} prior to the onset of spallation, and 160 kJ mol^{-1} in the post-spallation period. The pre-spallation kinetic data likely represent the superposition of U_3O_7 formation as well as both the nucleation and the growth of U_3O_8. The post-spallation activation energy reported by White et al. [24] likely corresponds to the formation of U_3O_8, but these data may have significant error associated with the change in surface area which occurs when powder formation begins.

You et al. [25] measured the weight gain of portions of LWR pellets and observed sigmoidal reaction curves. They estimated the activation energy for the formation of U_3O_8 on UO_2 to be 143 kJ mol^{-1} in the range 250–350°C and 109 kJ mol^{-1} in the range 350–400°C, using an Arrhenius plot of the time-to-50% reaction. Their results are thus comparable with the pseudo-activation energies reported by Boase and Vandergraaf [6] but are not directly comparable with the related work reported by White et al. [24].

Tucker [22] measured the rate of oxidation of portions of advanced gas-cooled reactor (AGR) pellets gravimetrically in controlled atmospheres (O_2 content varying between 0.1% and 27%). At temperatures below 500°C he found sigmoidal reaction kinetics. An activation energy for the post-induction period was determined by describing the reaction kinetics in terms of a maximum linear rate of weight gain, and using these data to construct an Arrhenius plot. The linear approximation to the sigmoidal reaction kinetics was found to give an activation energy of 170.2 kJ mol^{-1} in the range 200–300°C and 48.0 kJ mol^{-1} in the range 300–550°C. The results reported by Tucker [22] have significant errors because the rate of spalling of U_3O_8 from the sample surface affects the reaction kinetics and because linearity is a fairly poor approximation to the sigmoidal reaction kinetics.

Taylor et al. [7] studied the early stages of U_3O_8 formation on the surface of unirradiated UO_2 sintered pellets in the temperature range 200–300°C. They used XRD to determine the progress of U_3O_8 formation since this technique measures U_3O_8 specifically, i.e., without interference from the intermediate U_3O_7 phase. Arrhenius plots were made based on the time required for the production of 'minor' or 'detectable' amounts of U_3O_8, and these yielded estimates of 139 and 124 kJ mol^{-1} respectively. The results obtained by Taylor et al. were consistent with those obtained by Wheeler [26] who compiled weight-gain

[1] The nature of the product of the first stage of UO_2 oxidation varies depending on the oxidation conditions and the type of fuel. At low temperatures, spent light-water reactor (LWR) fuel, or UO_2 with high dopant levels oxidizes to a cubic U_4O_{9+y} phase, whereas unirradiated UO_2 oxidizes to tetragonal U_3O_7 [19,20]. For simplicity, we use the unqualified term 'U_3O_7' to refer to the product of the first stage of UO_2 oxidation.

data for irradiated CANDU [2] fragments from many sources. However, the experiments reported by Taylor et al. were semi-quantitative in nature. In the present paper we develop a model for quantitative analysis of the XRD data acquired by Taylor et al. and use these, and new data to determine an accurate activation energy for the formation of U_3O_8.

The focus of this paper is the determination of an accurate value of the activation energy for the formation of U_3O_8 at low (i.e., < 300°C) temperatures, since this is the range of interest for the dry storage of used nuclear fuel. We thus only mention briefly the activation energy of ca. 100 kJ mol^{-1} reported by Ohashi et al. [3] for the temperature range 300–450°C, and the value of 161.5 kJ mol^{-1} determined by Kissinger's method [27] for the range 365–400°C [28].

2.2. Used fuel

Several activation energies for the formation of U_3O_8 on used UO_2 fuel have been reported. Bennett et al. [29] measured the rate of weight gain of individual fragments of used AGR fuel. They did not report an activation energy but showed an Arrhenius plot with two linear regions-one region for 225–300°C and another from 350–400°C. The derived rate expressions correspond to activation energies of 155 kJ mol^{-1} and 81.0 kJ mol^{-1} respectively. You et al. [25] measured the rate of weight gain of individual used LWR fragments and reported an activation energy of 94.5 kJ mol^{-1} for the formation of U_3O_8 on UO_2 in the range 300–400°C. Hastings et al. [30,31] performed similar weight-gain experiments on fragments of both unirradiated and irradiated CANDU fuel. They claimed that a linear Arrhenius plot is valid over the range 175–400°C and suggested that deviations from linearity in previous work may be related to oxygen starvation at higher temperatures. Activation energies were estimated at 140 kJ mol^{-1} for unirradiated UO_2 and 120 kJ mol^{-1} for used CANDU fuel. However, it seems doubtful that their interpretation of linear Arrhenius behavior over such a wide temperature range is valid [6,21–23] and the importance they attach to oxygen starvation has been questioned [22,23]. Harrison et al. [5] oxidized irradiated polycrystalline UO_2 spheres and reported a burnup-dependent activation energy for the second stage of their oxidation reaction, but they were not convinced that the 'second stage' of their kinetic model necessarily corresponded to the reaction $U_3O_7 \rightarrow U_3O_8$. In the temperature range from 320–380°C they found an activation energy of 63 kJ mol^{-1} for low burnups, ranging up to 105 kJ mol^{-1} for high burnups (9 at.%). Einziger and Strain [32] oxidized used LWR fuel fragments in air in the range 250–360°C and recorded the time when spallation (associated with U_3O_8 formation) occurred. They found that the time-to-spallation displayed Arrhenius behavior with an activation energy of 194 ± 24 kJ mol^{-1}. However, it must be noted that this activation energy reflects the nucleation and growth of U_3O_8 as well as the energy required for the U_3O_8 to spall, i.e., to separate from the UO_2 substrate. Thus the activation energy of 194 kJ mol^{-1} is not directly comparable to values obtained for U_3O_8 nucleation and growth.

The oxidation of UO_2 proceeds by two stages (Eq. (3)) and the second stage involves both the nucleation and subsequent growth of U_3O_8. The overall reaction is thus complex, and there are potential problems with the application of weight-gain data to the study of reaction kinetics. For example, with unirradiated, sintered pellets, weight-gain data can be modelled with sigmoidal kinetics corresponding to the direct conversion from UO_2 to U_3O_8 [6,25] since there is only a thin layer of U_3O_7 formed at the reaction interface. In contrast, oxidation of used fuel (or unirradiated UO_2 powders) tends to display complex kinetics above 200°C because of the simultaneous formation of both U_3O_7 and U_3O_8 [4].

Estimation of the activation energy for the formation of U_3O_8 from weight-gain data is only valid if either the quantity of the intermediate U_3O_7/U_4O_9 is insignificantly small or the data are fitted to an expression that takes into consideration the complexity of the reaction. For used fuel, the approximation that the quantity of U_3O_7/U_4O_9 is small is of questionable validity at temperatures below 250°C since Thomas et al. [20] did not observe U_3O_8 in used LWR fuel samples oxidized below this temperature. In fact, low-temperature weight-gain curves for used-fuel fragments often plateau near 2% weight gain [25,32], which suggests complete conversion to U_3O_7/U_4O_9. Also, Wasywich et al. [10] noted that defected CANDU fuel rods oxidized at 150°C show substantial U_3O_7 but no detectable U_3O_8. We thus conclude that the low-temperature data of Bennett et al. [29] at 225–300°C and the data of Hastings et al. [31] likely represent the average of two different activation energies, i.e., for the formation of U_3O_7/U_4O_9 and also of U_3O_8 [33]. The high-temperature data of Bennett et al. [29], Harrison et al. [5] and You et al. [25] are likely more accurate than the low-temperature data, but it is still probable that the formation of U_3O_7/U_4O_9 introduces errors into such estimates of the activation energy for the growth of U_3O_8.

3. Theory

Previous estimates of the activation energy for the formation of U_3O_8 are unsatisfactory in many ways. Weight-gain data are susceptible to interference from the formation of U_3O_7/U_4O_9, especially for used fuel, which displays very rapid migration of oxygen along grain

[2] CANada Deuterium Uranium, registered trademark.

boundaries [33,34]. Pseudo-activation energies, calculated by a 'time-to-x%' reaction' model [6,25] are useful for empirical treatment of kinetic data, but do not provide insight into the fundamental process underlying the formation of U_3O_8. Many of the other studies imposed unrealistic constraints on the U_3O_8-formation kinetics, such as linear growth rate [22] or assumptions about the relative rates of nucleation and growth [13]. We have thus developed an improved approach, in which we measure specifically the rate of U_3O_8 formation, and analyze the kinetic data with a two-dimensional nucleation and growth model.

The progress of U_3O_8 formation on the surface of flat disks of UO_2 was monitored using XRD as described in Section 4. The kinetic data were then analyzed by comparison to a geometric model that considers the rate of nucleation (K_n, $m^{-2}\,h^{-1}$) and subsequent growth (at a rate of K_g, $m\,h^{-1}$) of circular U_3O_8 islands on a two-dimensional surface.

Several assumptions are implicit in the model developed herein:

– that the rate of growth of U_3O_8 is isotropic, so that the nuclei spread to form circular islands.

– that a two-dimensional model can be used to describe U_3O_8 formation on the surface of a three-dimensional disk. We accept this assumption because the sampling depth of XRD on a UO_2 surface is small (< 1 μm) relative to the size of the sample, which was a flat, circular disk of diameter ~ 1.1 cm, and the grain size (10 μm)..

– that the grain structure of the UO_2 sintered disks does not affect the growth of the circular islands. The grain diameter in CANDU fuel is typically 10 μm, and there is evidence of preferred-orientation effects in U_3O_8 formation [7]; thus the grain structure may have had an impact on the deviations between calculated and experimental reaction kinetics (Section 5).

3.1. Geometric analysis of two-dimensional nucleation-and-growth kinetics

Consider the growth of U_3O_8 on a two-dimensional UO_2 surface [3]. We assume that the U_3O_8 forms initially as microscopic nuclei, which then grow as circular islands until they eventually cover the entire flat surface. We define K_g ($m\,h^{-1}$) as the isotropic rate constant for the linear rate of U_3O_8 growth. The area, $A(t, \tau)$, at time t of a U_3O_8 island, which had nucleated previously at time τ, is given by

$$A(t, \tau) = \pi\left[K_g(t-\tau)\right]^2. \tag{4}$$

If a surface contains N such islands at time t, then we define a dimensionless number $\alpha'(t)$ as the sum of the areas of all islands that nucleated prior to time t divided by the total area of the surface F,

$$\alpha'(t) = \frac{1}{F}\sum_{\substack{i=1\\ \tau_i<t}}^{N} A(t, \tau_i) = \frac{1}{F}\sum_{\substack{i=1\\ \tau_i<t}}^{N} \pi\left[K_g(t-\tau_i)\right]^2. \tag{5}$$

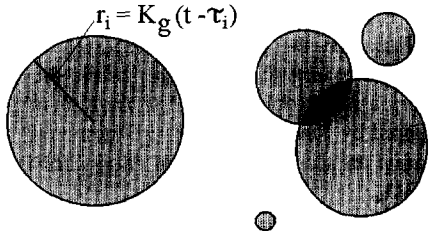

Fig. 1. Growth of circular U_3O_8 islands on a two-dimensional flat UO_2 surface. The sum of the area of all the circles (shaded grey) is equal to $\alpha'(t)$, and the function $\alpha(t)$ is equal to the fraction of the surface converted to U_3O_8. Thus for calculation of $\alpha'(t)$ the area shaded dark grey is counted twice, whereas for $\alpha(t)$ it is only included once.

The fraction of the surface covered by U_3O_8 at time, t, will in general be less that $\alpha'(t)$, because of overlap between various U_3O_8 islands. We thus define $\alpha(t)$ as the actual fraction of the surface converted to U_3O_8. Thus for calculation of $\alpha(t)$ the areas of overlap between neighboring U_3O_8 islands are only included once, whereas for calculation of $\alpha'(t)$ they are included two (or more) times. The growth of U_3O_8 islands on a two-dimensional surface of UO_2 is illustrated in Fig. 1.

The number of nuclei formed at time τ on the entire surface is defined as $n(\tau)$, and the rate of nuclei formation is thus the time derivative of $n(\tau)$. We assume that the rate of nucleation is proportional to the area unconverted to U_3O_8 product, i.e.,

$$\frac{dn(\tau)}{d\tau} = K_n F\left[1-\alpha(\tau)\right], \tag{6}$$

where K_n is the nucleation rate constant per unit area. The number of nuclei formed between time τ and $\tau + d\tau$ is then given by $dn(\tau)$,

$$dn(\tau) = K_n F\left[1-\alpha(\tau)\right]d\tau. \tag{7}$$

Assuming that the growth of U_3O_8 nuclei starts at time $\tau = 0$, we can now replace the discrete sum in Eq. (5) by a continuous integral, and write

$$\alpha'(t) = \frac{1}{F}\int_{\tau=0}^{t} dn(\tau)\, A(t, \tau) = \frac{1}{F}\int_{\tau=0}^{t} dn(\tau)\, \pi\left[K_g(t-\tau)\right]^2. \tag{8}$$

Using Eq. (7) gives

$$\alpha'(t) = \pi K_g^2 K_n \int_{\tau=0}^{t}\left[1-\alpha(\tau)\right](t-\tau)^2\, d\tau. \tag{9}$$

To simplify Eq. (9) we need an expression that relates

[3] The sample will, in fact, have a thin surface layer of U_3O_7, but the experiments reported herein measure the formation of U_3O_8 specifically; thus the degree of conversion from UO_2 to U_3O_7 will not have a significant impact on the observed U_3O_8-formation kinetics.

$\alpha(t)$ to $\alpha'(t)$. The generally accepted approximation is [35]

$$1-\alpha(t)=\mathrm{e}^{-\alpha'(t)}. \tag{10}$$

Eq. (10) displays the appropriate behavior under the limiting conditions

$$\alpha(t)\sim\alpha'(t) \quad \text{for } 0<t\ll 1,$$
$$\alpha(t)=1 \quad \text{at } t=\infty$$

Substituting Eq. (10) into Eq. (9) yields

$$\alpha'(t)=\pi K_g^2 K_n\int_{\tau=0}^{t}(t-\tau)^2\mathrm{e}^{-\alpha'(\tau)}\,\mathrm{d}\tau. \tag{11}$$

Differentiation of Eq. (11) three times with respect to time yields

$$\frac{\mathrm{d}\alpha'(t)}{\mathrm{d}t}=2\pi K_g^2 K_n\int_{\tau=0}^{t}(t-\tau)\mathrm{e}^{-\alpha'(\tau)}\,\mathrm{d}\tau, \tag{12}$$

$$\frac{\mathrm{d}^2\alpha'(t)}{\mathrm{d}t^2}=2\pi K_g^2 K_n\int_{\tau=0}^{t}\mathrm{e}^{-\alpha'(\tau)}\,\mathrm{d}\tau \tag{13}$$

and

$$\frac{\mathrm{d}^3\alpha'(t)}{\mathrm{d}t^3}=2\pi K_g^2 K_n\mathrm{e}^{-\alpha'(\tau)}, \tag{14}$$

where, in the first two differentiations, use was made of the relation, valid for any functions f, p and q of the variables x and a,

$$\frac{\mathrm{d}}{\mathrm{d}a}\int_p^q f(x,a)\,\mathrm{d}x=\int_p^q\frac{\partial}{\partial a}[f(x,a)]\,\mathrm{d}x+f(q,a)\frac{\mathrm{d}q}{\mathrm{d}a}-f(p,a)\frac{\mathrm{d}p}{\mathrm{d}a} \tag{15}$$

and in the last one

$$\frac{\mathrm{d}}{\mathrm{d}a}\int_0^a f(x)\,\mathrm{d}x=f(a), \tag{16}$$

which is a special case of Eq. (15).

The differential Eq. (14) cannot be solved explicitly; thus it is solved by use of an infinite series. We assume that the function $\alpha'(t)$ can be described by an infinite Taylor series,

$$\alpha'(t)=\sum_{k=0}^{\infty}c_k t^k. \tag{17}$$

Differentiating Eq. (17) repeatedly with respect to time yields

$$\frac{\mathrm{d}^3\alpha'(t)}{\mathrm{d}t^3}=\sum_{k=0}^{\infty}\frac{(k+3)!}{k!}c_{k+3}t^k. \tag{18}$$

The exponential term on the right-hand side of Eq. (14) can be expanded as an infinite series,

$$\frac{\mathrm{d}^3\alpha'(t)}{\mathrm{d}t^3}=2\pi K_g^2 K_n\sum_{j=0}^{\infty}\frac{(-1)^j}{j!}\alpha'^j(t). \tag{19}$$

Substitution of Eq. (17) for $\alpha'(t)$ into the right-hand side of Eq. (19) gives

$$\frac{\mathrm{d}^3\alpha'(t)}{\mathrm{d}t^3}=2\pi K_g^2 K_n\sum_{j=0}^{\infty}\frac{(-1)^j}{j!}\left\{\sum_{k=0}^{\infty}c_k t^k\right\}^j. \tag{20}$$

The right-hand side of Eq. (20) can be expanded,

$$\begin{aligned}\frac{\mathrm{d}^3\alpha'(t)}{\mathrm{d}t^3}&=2\pi K_g^2 K_n\left\{1-\sum_{k=0}^{\infty}c_k t^k+\frac{1}{2!}\sum_{l=0}^{\infty}\sum_{k=0}^{\infty}c_l c_k t^{k+l}\right.\\&\quad-\frac{1}{3!}\sum_{m=0}^{\infty}\sum_{l=0}^{\infty}\sum_{k=0}^{\infty}c_m c_l c_k t^{k+l+m}\\&\quad\left.+\frac{1}{4!}\sum_{n=0}^{\infty}\sum_{m=0}^{\infty}\sum_{l=0}^{\infty}\sum_{k=0}^{\infty}c_n c_m c_l c_k t^{k+l+m+n}+\dots\right\}.\end{aligned} \tag{21}$$

Equating Eqs. (18) and (21) yields

$$\begin{aligned}\sum_{k=0}^{\infty}\frac{(k+3)!}{k!}c_{k+3}t^k&=2\pi K_g^2 K_n\left\{1-\sum_{k=0}^{\infty}c_k t^k+\frac{1}{2!}\sum_{l=0}^{\infty}\sum_{k=0}^{\infty}c_l c_k t^{k+l}\right.\\&\quad-\frac{1}{3!}\sum_{m=0}^{\infty}\sum_{l=0}^{\infty}\sum_{k=0}^{\infty}c_m c_l c_k t^{k+l+m}\\&\quad\left.+\frac{1}{4!}\sum_{n=0}^{\infty}\sum_{m=0}^{\infty}\sum_{l=0}^{\infty}\sum_{k=0}^{\infty}c_n c_m c_l c_k t^{k+l+m+n}+\dots\right\}.\end{aligned} \tag{22}$$

We next compare terms of equal order in t on the left- and right-hand sides of Eq. (22) to solve for the coefficients, c_k, of the polynomial expression of $\alpha'(t)$. First we note that Eq. (17) and the initial condition $\alpha'(t=0)=0$ implies $c_0=0$. Similarly, from Eqs. (12) and (13) we have two further initial conditions,

$$\frac{\mathrm{d}\alpha'(t=0)}{\mathrm{d}t}=\frac{\mathrm{d}^2\alpha'(t=0)}{\mathrm{d}t^2}=0, \tag{23}$$

giving $c_1=c_2=0$. Equating the t^0 terms in Eq. (22) then gives

$$1\cdot 2\cdot 3\cdot c_3=2\pi K_g^2 K_n,\quad c_3=\frac{\pi K_g^2 K_n}{3}. \tag{24}$$

Comparison of terms of order t^1 and t^2 in Eq. (22) shows that $c_4=c_5=0$. Equating the t^3 terms gives

$$4\cdot 5\cdot 6\cdot\left(c_6 t^3\right)=-2\pi K_g^2 K_n c_3 t^3,$$

$$c_6=\frac{-\left(\pi K_g^2 K_n\right)^2}{180}. \tag{25}$$

Further analysis of Eq. (22) allows one to determine

$$c_7 = c_8 = 0, \tag{26}$$

$$c_9 = \frac{11\left(\pi K_g^2 K_n\right)^3}{45\,360}, \tag{27}$$

$$c_{10} = c_{11} = 0, \tag{28}$$

$$c_{12} = -\frac{5\left(\pi K_g^2 K_n\right)^4}{399\,168}. \tag{29}$$

Truncating the infinite series in Eq. (17) after 12 terms we obtain a relation for $\alpha'(t)$,

$$\alpha'(t) = \frac{\pi K_g^2 K_n t^3}{3} - \frac{\left(\pi K_g^2 K_n t^3\right)^2}{180} + \frac{11\left(\pi K_g^2 K_n t^3\right)^3}{45\,360} - \frac{5\left(\pi K_g^2 K_n t^3\right)^4}{399\,168}. \tag{30}$$

and using Eqs. (10) and (30) we obtain an expression for $\alpha(t)$,

$$\alpha(t) = 1 - \exp\left\{ - \frac{\pi K_g^2 K_n t^3}{3} + \frac{\left(\pi K_g^2 K_n t^3\right)^2}{180} - \frac{11\left(\pi K_g^2 K_n t^3\right)^3}{45\,360} + \frac{5\left(\pi K_g^2 K_n t^3\right)^4}{399\,168} \right\}. \tag{31}$$

For simplicity, we introduce the variable κ, defined by

$$\kappa = K_g^2 K_n, \tag{32}$$

which then simplifies Eq. (31) to

$$\alpha(t) = 1 - \exp\left\{ - \frac{\pi \kappa t^3}{3} + \frac{\pi^2 \kappa^2 t^6}{180} - \frac{11\pi^3 \kappa^3 t^9}{45\,360} + \frac{5\pi^4 \kappa^4 t^{12}}{399\,168} \right\}. \tag{33}$$

To illustrate the validity of the truncated infinite series used in the derivation of Eq. (33), numerical integration was used to obtain exact solution of the differential Eq. (14) for $\kappa = 10^{-6}$ s^{-3}. The resulting expression for $\alpha'(t)$ was converted to a relation for $\alpha(t)$ by use of Eq. (10). The resulting exact solution for $\alpha(t)$ is compared with a plot of $\alpha(t)$ obtained by use of Eq. (33) in Fig. 2. Examination of Fig. 2 shows that Eq. (33) is an excellent approximation to the exact solution up to values of $\alpha(t) > 0.90$. Eq. (33) is therefore acceptable for the present work, since UO_2 disks that undergo a high degree of surface oxidation (i.e., $\alpha > \sim 0.5$) tend to have U_3O_8 spalling from the surface. Experience has shown that such samples are difficult to work with from a radiological protection point of view; moreover, they yield erratic XRD data. Thus, only those samples with values of $\alpha(t) \leq 0.5$ were used in the data analysis reported herein. An alternative approach could be to include a term in Eq. (8) which accounts for U_3O_8 spalling.

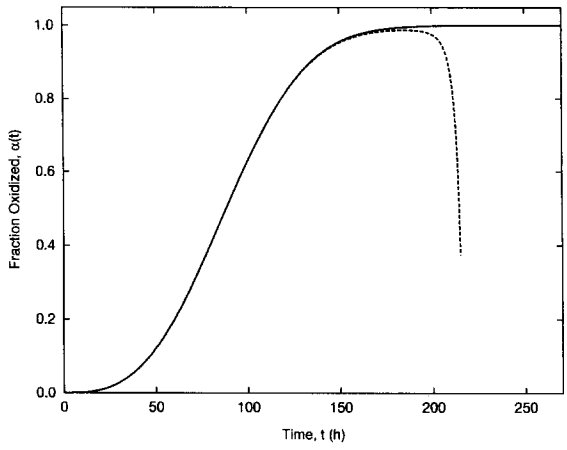

Fig. 2. Exact solution to Eq. (14) (solid line) compared with the approximate solution (dashed line) obtained by use of Eq. (33).

Eq. (33) is consistent with the analogous three-dimensional nucleation-and-growth models, which are a function of time and the product $K_g^3 K_n$ [15,36].

3.2. The two-dimensional finite-element method

A finite-element FORTRAN code was written to check the validity of the geometrical model derived above, specifically, to ensure that the approximate expression (Eq. (10)), which relates $\alpha(t)$ to $\alpha'(t)$ is legitimate.

The FORTRAN model consists of a $p \times p$ square array of points which represents the UO_2 surface to be oxidized. To account for edge effects, the p^2 grid is located in the center of a larger $q \times q$ grid ($q > p$). Typical values of p and q were 2000 and 2200, respectively. In the model, U_3O_8 nucleates and grows on the entire $q \times q$ grid, but only the central $p \times p$ region is sampled to determine the degree of oxidation, i.e., $\alpha(t)$.

Inputs for the code include the rates of U_3O_8 nucleation, K_n (h^{-1} m^{-2}) and growth, K_g (m h^{-1}). Initially, the entire $q \times q$ grid is defined to consist of UO_2 points. The code models nucleation by converting finite elements of the grid to U_3O_8 in time intervals of $1/K_n$ (i.e., 1 nucleus is formed per cycle). Each cycle, one location in the $q \times q$ grid (i.e., including the boundary area) is selected for nucleation by a random number generator. If the selected element is within a region already converted to U_3O_8, then no nucleus is placed on the model surface during that cycle. If the site chosen is UO_2, then that element is converted to U_3O_8, and information about its location and age is stored.

The nucleation-and-growth process continues over the flat surface (defined to be of magnitude 1 m^2) in $1/K_n$ (h) time increments, and the surface area coverage, $\alpha(t)$, is calculated at selected intervals during the course of the reaction. To determine $\alpha(t)$, the radius of each circular island is calculated by taking the product of the U_3O_8 growth rate (K_g, m h^{-1}) and the time elapsed since

nucleation of that U_3O_8 island (the code records the location of each nucleation site, as well as the time it was formed). Tabulation of the elements converted to U_3O_8 is accomplished by constructing a square grid around each U_3O_8 island in turn. Each finite element within the square is then examined to determine whether or not it is within (or on the boundary of) the circular disk associated with the U_3O_8 island. If the finite element is within the U_3O_8 island, then the number of U_3O_8 elements is incremented accordingly, unless the element had been already counted as U_3O_8 during examination of a previous island. The tabulation routine is thus able to eliminate duplicate tabulation of finite elements because of overlap of two or more U_3O_8 islands (Fig. 1). After examination of all U_3O_8 islands, the number of U_3O_8 elements tabulated is compared with the number of remaining UO_2 elements, and the fraction, $\alpha(t)$ of surface oxidized is calculated.

3.3. Comparison of geometric and finite-element methods

A series of tests was performed to compare the finite-element method with the geometric model described by Eq. (33) to check the validity of the assumption described by Eq. (10). Eq. (33) does not depend on K_g or K_n individually, but rather it is a function of the product $\kappa = K_g^2 K_n$. We thus expect that reaction curves calculated by the finite-element code should coincide with the geometric-model results for all combinations of K_n and K_g values that yield the same κ value from Eq. (32). Several constant-κ reaction curves were calculated by the finite-element model and good agreement was obtained with curves obtained by Eq. (33). A typical comparison between finite-element and geometric models is given in Fig. 3.

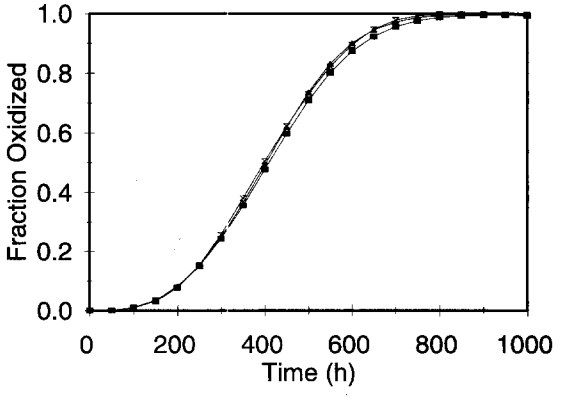

Fig. 3. Fraction of the surface converted to U_3O_8 as a function of time for constant values of $\kappa = K_g^2 K_n$, as calculated using Eq. (33) and the finite-element code. Symbols represent: (■) Eq. (33) with $K_g = 0.0001$ m h^{-1}, $K_n = 1$ m^{-2} h^{-1}; (⋈) finite-element code with $K_g = 0.0003162$ m h^{-1} and $K_n = 0.1$ m^{-2} h^{-1}; (▲) finite-element code with $K_g = 0.00003162$ m h^{-1} and $K_n = 10$ m^{-2} h^{-1}.

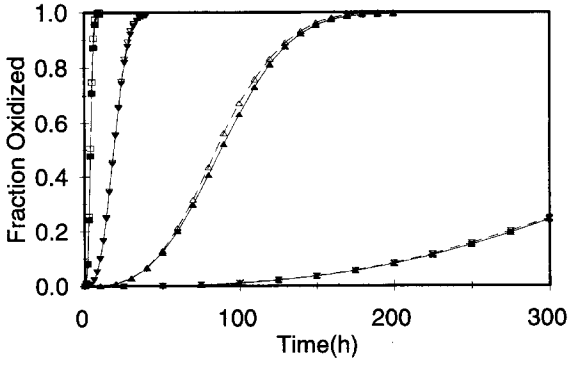

Fig. 4. Fraction, $\alpha(t)$, of the surface converted to U_3O_8 as a function of time, as calculated by Eq. (33) (hollow symbols, dashed lines) and by the finite-element code (solid symbols and lines). Values of K_g (m h^{-1}) and K_n (m^{-2} h^{-1}) respectively were: (⋈) (0.0001, 1); (△) (0.001, 1); (▽) (0.003162, 10); (□) (0.01, 100).

To confirm that there is good agreement between the two methods over a range of κ values, reaction curves were calculated by both the geometric and the finite-element methods for reaction times varying between 10 and 1000 h. The agreement between the two methods was generally good (Fig. 4). The average deviation between data points calculated by the different methods was 0.00025 for the four reaction curves shown in Fig. 4. The only systematic difference between the two methods was that the finite-element method generally gave slightly higher results than the geometric model when the fraction converted was in the range 0.6–0.9. This error is deemed to be associated with the approximate relation between $\alpha'(t)$ and $\alpha(t)$ given in Eq. (10). Errors introduced by use of the approximate relation (Eq. (10)) are not significant relative to sample-to-sample variation in the rate of U_3O_8 formation because U_3O_8 nucleation is a sensitive function of surface preparation [7].

We concluded that either the finite-element or the geometric method can be used for our data analysis. For simplicity, our experimental data were fitted to Eq. (33) using a routine which varied the value of κ to obtain the minimum sum of the squares of deviations between experimental and calculated $\alpha(t)$ values.

4. Experimental

Samples used to measure the rate of U_3O_8 growth as a function of time and temperature were cut from unirradiated CANDU fuel pellets, which have an average grain size of ~ 10 μm. Since the rate of U_3O_8 formation is dependent on the roughness of polished UO_2 surfaces [7,37], each of the specimens was ground to a 400-grit finish. The samples were then oxidized in the range 168–300°C in unlimited laboratory air in electric tube furnaces,

which have temperature control to within ±2°C. In some cases the samples were only oxidized and analyzed once, and then the experiment was terminated. In other cases the samples underwent a series of heating/cooling/analysis cycles sequentially, until the surface was greater than 50% oxidized. It was necessary to perform such a cyclical procedure since the XRD apparatus cannot be heated above room temperature. Tests have shown that thermal cycling does not have a significant impact on the rate of U_3O_8 formation on unirradiated UO_2 [38]. Further details of the oxidation experiments have been published elsewhere [7]. The data used in the current analysis include those presented, and semi-quantitatively analyzed in Ref. [7].

The rate of U_3O_8 formation was measured by XRD using a Rigaku Rotaflex diffractometer operating with a 12 kW Cu Kα source. The diffractometer scanning rate was $10°\ (2\theta)\ \text{min}^{-1}$.

As discussed in an earlier publication [39] the fraction, $\alpha(t)$, of U_3O_8 present on the surface of a UO_2 disk can be calculated by comparison of the intensity of the XRD peaks associated with U_3O_8 relative to the intensity of those associated with U_3O_7 [4]. The fraction of the surface (i.e., within the effective XRD sampling depth of < 1 μm) oxidized to U_3O_8 at a given time is given by

$$\alpha(t) = \frac{I_{U_3O_8}}{I_{U_3O_8} + \xi \cdot I_{U_3O_7}}, \tag{34}$$

where $I_{U_3O_8}$ is the integrated intensity of the U_3O_8 peak at $d = 0.34$ nm, $I_{U_3O_7}$ is that of the U_3O_7 peak at $d = 0.31$ nm, and ξ is an empirically determined factor which corrects for the different absolute XRD intensities and mass absorption coefficients of U_3O_8 and U_3O_7. Measurement of ξ was accomplished by measuring the intensities of $I_{U_3O_8}$ and $I_{U_3O_7}$ for a series of identical UO_2 disks oxidized at 250°C for varying lengths of time and was found to be 0.450 ± 0.033 [39].

5. Results and discussion

5.1. Analysis of experimental data

The integrated intensity ($I_{U_3O_8}$) of the U_3O_8 peak at $2\theta \sim 26.0°$ and the intensity ($I_{U_3O_7}$) of the U_3O_7 peak at $2\theta \sim 28.5°$ were measured from the XRD spectra of each sample after heat treatment. The fraction, $\alpha(t)$, of the surface converted to U_3O_8 was then calculated by use of Eq. (34). The average rate constant, κ (Eq. (32)) was calculated for each oxidation dataset by fitting the experimental data to Eq. (33). For each dataset the origin was included as a data point since XRD analysis of polished samples prior to heat treatment consistently displayed no significant quantity of U_3O_8. The validity of Eq. (33) is illustrated by comparison with experimental data in Fig. 5. To facilitate comparison of all experimental data with Eq. (33) the values of time in Fig. 5 have been calculated in terms of the reduced time, i.e., the ratio $t/t_{1/2}$ where $t_{1/2}$ is the time required to achieve 50% reaction. The individual values of the data points in Fig. 5 cannot be compared to the curve, because the values of κ displayed in this figure were calculated by empirical fit to Eq. (33). However, there is good agreement between the shape of the curve and the pattern of the data points, which suggests validity of our model (Eq. (33)). The experimentally determined values of $I_{U_3O_8}$ and $I_{U_3O_7}$, along with the calculated values of $\alpha(t)$ and κ are given in Table 2.

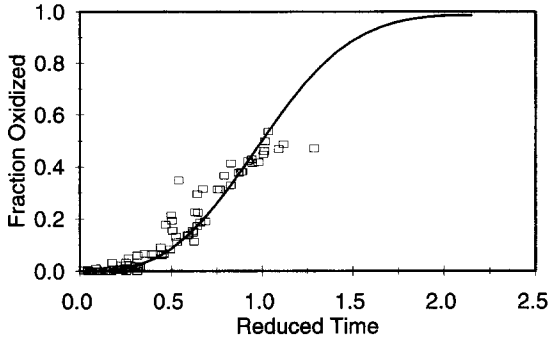

Fig. 5. Experimental data (Table 2) for the fraction of the surface converted to U_3O_8 as a function of reduced time (i.e., $t/t_{1/2}$, where $t_{1/2}$ is the time required to achieve 50% reaction.

5.2. Determination of the activation energy for U_3O_8 formation

The values of the average rate constant (κ) given in Table 2 were used to construct an Arrhenius plot for the formation of U_3O_8 on UO_2 disks. The Arrhenius plot (Fig. 6) did not display significant deviations from linearity over the temperature range 168–300°C. A linear regression was performed on the kinetic data, with each value of κ weighted according to the square root of the number of non-zero points in the corresponding data set. The linear regression of the Arrhenius plot yielded the relationship

$$\ln \kappa = (-52\,808 \pm 3{,}442)\frac{1}{T} + 86.165, \tag{35}$$

where the reported uncertainty is the 90% confidence interval in the slope. The activation energy for U_3O_8 formation is thus

$$E_a = (52\,808 \pm 3{,}442)\frac{8.3145\ \text{J mol}^{-1}\ \text{K}^{-1}}{3}, \tag{36}$$

$$E_a = 146 \pm 10\ \text{kJ mol}^{-1}, \tag{37}$$

[4] By the time significant U_3O_8 forms on the sample surface, the underlying UO_2 is covered with a layer of U_3O_7.

Table 2
Intensity of the U_3O_7 and U_3O_8 XRD peaks, the fraction [$\alpha(t)$] of the surface oxidized, and the average rate constant (κ) for UO_2 disks heated various lengths of time in unlimited laboratory air

Temp (°C)	Time (h)	$I_{U_3O_8}$	$I_{U_3O_7}$	$\alpha(t)$	κ (h^{-3})
300	2.0	190	12265	0.0333	1.37×10^{-3}
	4.0	1145	10673	0.1924	
	6.0	2011	9777	0.3135	
	8.0	3180	8703	0.4479	
300	2.0	10275	358775	0.0598	2.69×10^{-3}
	4.0	41444	315729	0.2257	
	6.0	97186	304062	0.4151	
300	1.0	0	538671	0.0000	2.61×10^{-3}
	1.5	1287	525098	0.0054	
	2.0	0	577466	0.0000	
	3.0	46170	473374	0.1780	
	4.0	26990	472422	0.1126	
295	3.0	25895	315693	0.1541	5.97×10^{-3}
288	6.0	91185	276788	0.4225	2.49×10^{-3}
275	7.0	0	376777	0	3.22×10^{-5}
	15.0	64021	266930	0.3475	
	23.0	73474	231311	0.4136	
	31.0	50665	118380	0.4873	
275	17.6	69830	337153	0.3150	3.85×10^{-5}
	25.6	98156	304269	0.4173	
	33.6	116349	289494	0.4716	
275	8.0	956	11569	0.1550	1.75×10^{-4}
	16.0	3649	8137	0.4989	
275	4.0	0	375909	0.0000	5.51×10^{-5}
	24.0	142099	272735	0.5364	
275	8.0	10593	340968	0.0645	8.13×10^{-5}
	18.0	80388	289926	0.3811	
265	18.0	27736	389146	0.1366	2.42×10^{-5}
263	18.0	38778	411109	0.1732	3.14×10^{-5}
260	8.0	74	13484	0.0120	9.30×10^{-7}
	16.0	204	13699	0.0320	
	24.0	186	7940	0.0494	
	32.0	233	7211	0.0669	
	40.0	332	7396	0.0906	
	48.0	431	7637	0.1114	
	56.0	615	7945	0.1467	
	62.0	770	7298	0.1898	
255	18.0	25	4871	0.0113	1.86×10^{-6}
250	80	45063	366736	0.2144	1.66×10^{-7}
	103.2	66294	351748	0.2950	
	127.2	81126	312589	0.3656	
	151.2	103612	304921	0.4300	
	175.2	111985	281208	0.4693	
250	79.2	14156	444251	0.0661	9.01×10^{-8}
	103.2	26533	390485	0.1311	
	127.2	44169	341495	0.2231	
	151.2	65265	319328	0.3122	
	175.2	80232	288423	0.3818	
	199.2	102310	264918	0.4616	
250	24.0	113	13177	0.0187	1.78×10^{-6}
	48.0	1105	10750	0.1858	
245	54.0	54614	247134	0.3292	2.47×10^{-6}
240	100	80	2509	0.0661	6.60×10^{-8}
230	100	194	2737	0.1360	1.41×10^{-7}

Table 2 (continued)

Temp (°C)	Time (h)	$I_{U_3O_8}$	$I_{U_3O_7}$	$\alpha(t)$	κ (h^{-3})
225	24.0	24	13289	0.0040	5.10×10^{-10}
	48.0	30	13282	0.0050	
	72.0	0	13035	0.0000	
	168	0	7712	0.0000	
	240	27	8092	0.0074	
	336	76	8117	0.0204	
225	120	0	616254	0.0000	6.05×10^{-11}
	264	0	417070	0.0000	
	504	4253	418105	0.0221	
	1008	11351	389514	0.0608	
225	48.0	0	3500	0.0000	3.09×10^{-9}
	96.0	0	3500	0.0000	
	192	20	3596	0.0122	
	360	232	3133	0.1412	
210	480	151	3701	0.0831	7.52×10^{-10}
210	480	492	1805	0.3772	4.09×10^{-9}
200	120	0	1	0.0000	9.50×10^{-11}
	192	0	1	0.0000	
	288	0	1	0.0000	
	480	19	3644	0.0115	
200	347.5	0	8227	0.0000	1.64×10^{-12}
	710.5	0	7757	0.0000	
	1046.5	9	9233	0.0022	
	1382.5	35	8814	0.0087	
168	9406			0.0105	1.21×10^{-14}
168	9406			0.0104	1.20×10^{-14}
168	9406			0.0066	7.60×10^{-15}

where the factor 3 in Eq. (36) was introduced because the rate constant κ represents the cube of the weighted average of the rate constants for nucleation and growth, as defined in Eq. (32). The activation energy reported herein is in reasonable agreement with the related values (124, 139 kJ mol^{-1}) published earlier by Taylor et al. [7].

We recognize that there is no theoretical justification for displaying our kinetic data as an Arrhenius plot because nucleation need not display Arrhenius behavior.

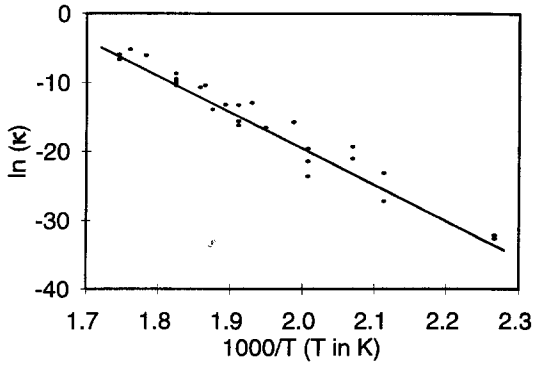

Fig. 6. Arrhenius plot for the average rate constant (κ) for the formation of U_3O_8 on UO_2. The fitted line corresponds to Eq. (35).

Table 3
Extrapolated estimates of the rate constant κ and the time required to reach $\alpha(t) = 0.015$ for several temperatures

Temperature (°C)	κ (h^{-3})	Time to reach $\alpha(t) = 0.015$ (h)
100	9.12×10^{-25}	2.51×10^{7}
150	1.67×10^{-17}	9.53×10^{4}
170	4.66×10^{-15}	1.46×10^{4}

However, the linearity of the data in Fig. 6 is convincing so that we believe our method is a legitimate first step in an effort to obtain realistic estimates of the rate of air oxidation of U_3O_8. Experiments are currently being performed to deconvolute the rate of U_3O_8 nucleation from its subsequent growth; we hope to publish these data at a later date.

5.3. Implications for dry air storage of used nuclear fuel

The results presented herein can be used to estimate the time required for formation of U_3O_8 on used nuclear fuel in dry air storage. Our data can be conservatively applied to used CANDU fuel because experiments have shown that the rate of U_3O_8 formation is somewhat inhibited by the presence of fission products in the fuel [39]. For a given temperature, the rate constant κ was calculated using Eq. (35) and the fraction of the surface oxidized to U_3O_8 was then calculated as a function of time using Eq. (33). We then assumed that the rate of bulk (i.e., three-dimensional) oxidation of a UO_2 sample is the same as that of the rate of U_3O_8 formation on the surface of a similar sample; clearly this is a conservative assumption because the rate of U_3O_8 growth into a UO_2 particle will probably be less than two-dimensional growth along the surface.

Eqs. (33) and (35) were used to calculate the time required for conversion of 1.5% (i.e., $\alpha(t) = 0.015$) of the sample surface to U_3O_8 at 170, 150 and 100°C. Transformation of 1.5% of the sample surface to U_3O_8 was chosen for these calculations because it represents one-tenth of the degree of reaction required to cause sheath splitting in defected fuel elements [31]. The results of such calculations are shown in Table 3.

6. Conclusions and suggestions for further work

A novel method has been presented to analyze quantitatively nucleation-and-growth kinetics by measuring the rate of product formation by XRD on a flat surface. The quantitative method was used to analyze the kinetic data for the formation of U_3O_8 on the surface of UO_2 disks over the range 168–300°C. The resulting Arrhenius plot did not deviate significantly from linearity, which suggests that nucleation and growth have similar activation energies in the temperature range studied. The activation energy for U_3O_8 formation was found to be 146 ± 10 kJ mol^{-1}. The quantitative procedure developed herein was used to conservatively estimate that the time for splitting to occur in a defected fuel element will be > 10.9 years in dry air storage at 150°C for a low burnup fuel (modelled using unirradiated UO_2).

The method presented herein uses XRD to measure specifically the rate of formation of U_3O_8 on the surface of UO_2 samples. The kinetic data are thus not prone to errors associated with the first stage of oxidation (i.e., formation of U_3O_7/U_4O_9), as is the case with weight-gain experiments. The current model can be improved by taking into account the grain structure of the UO_2 and the possible non-Arrhenius behavior of the U_3O_8 nucleation process.

It would be most useful to perform an experiment in which the present method was applied to the oxidation of used fuel. Such a test would lead to a significantly improved estimate of the time required for U_3O_8 formation on used fuel.

Acknowledgements

The authors appreciate critical review of this manuscript by S. Mezyk and C. Wren.

References

[1] P.E. Blackburn, J. Weissbart, E.A. Gulbransen, J. Phys. Chem. 652 (1958) 902.
[2] S. Aronson, in: Uranium Dioxide: Properties and Nuclear Applications, ed. J. Belle (US Atomic Energy Commission, Washington, DC, 1961).
[3] H. Ohashi, H. Hayashi, M. Nabeshima, T. Morozumi, Bull. of the Faculty of Engineering, Hokkaido University, No. 134, 1987.
[4] S. Aronson, R.B. Roof Jr., J. Belle, J. Chem. Phys. 27 (1957) 137.
[5] K.T. Harrison, C. Padgett, K.T. Scott, J. Nucl. Mater. 23 (1967) 121.
[6] D.G. Boase, T.T. Vandergraaf, Nucl. Technol. 32 (1977) 60.
[7] P. Taylor, D.D. Wood, A.M. Duclos, J. Nucl. Mater. 189 (1992) 116.
[8] K.A. Simpson, P. Wood, eds., Proc. Workshop on Chemical Reactivity of Oxide Fuel and Fission Product Release, held at Berkeley Nuclear Laboratories, Apr. 1987 (Central Electricity Generating Board, UK, Technology Planning and Research Division, 1987).
[9] R.E. Woodley, R.E. Einziger, H.C. Buchanan, Nucl. Technol. 85 (1989) 74.
[10] K.M. Wasywich, W.H. Hocking, D.W. Shoesmith, P. Taylor, Nucl. Technol. 104 (1993) 309.
[11] J. Novak, I.J. Hastings, E. Mizzan, R.J. Chenier, Nucl. Technol. 63 (1983) 254.
[12] R.E. Einziger, J.A. Cook, Nucl. Technol. 69 (1985) 55.
[13] D.E.Y. Walker, J. Appl. Chem. 15 (1965) 128.

[14] Y. Saito, Nippon Kinzoku Gakkaishi 39 (1975) 760.
[15] W.A. Johnson, R.F. Mehl, Trans. Am. Inst. Min. (Metall.) Eng. 135 (1939) 416.
[16] M. Avrami, J. Chem. Phys. 7 (1939) 1103.
[17] M. Avrami, J. Chem. Phys. 8 (1940) 212.
[18] B.V. Erofeev, C.R. Acad. Sci. URSS 52 (1946) 5111.
[19] P. Taylor, E.A. Burgess, D.G. Owen, J. Nucl. Mater. 88 (1980) 153.
[20] L.E. Thomas, R.E. Einziger, H.C. Buchanan, J. Nucl. Mater. 201 (1993) 310.
[21] K.A. Simpson, P. Wood, Proc. of the US Nuclear Regulatory Commission, Workshop on Spent Fuel/Cladding Reaction During Dry Storage, Gaithersburg MD, 1983, p. 70.
[22] P.M. Tucker, in: Proc. Workshop on Chemical Reactivity on Oxide Fuel and Fission Product Release, Berkeley, UK, eds. K.A. Simpson and P. Wood (CEGB, London, 1987) p. 49.
[23] P. Wood, G.G. Bannister, in: Proc. Workshop on Chemical Reactivity on Oxide Fuel and Fission Product Release, Berkeley, UK, eds. K.A. Simpson and P. Wood (CEGB, London, 1987) p. 19.
[24] G.D. White, C.A. Knox, E.R. Gilbert, A.B. Johnson, Jr., Proc. of a US Nuclear Regulatory Commission Workshop on Spent Fuel/Cladding Reaction During Dry Storage, held in Gaithersburg, MD, 1983, p. 102.
[25] G.-S. You, K.-S. Kim, S.-G. Ro, E.-K. Kim, Proc. of the JAERI-KAERI Joint Seminar on Post Irradiation Examination, held in Oarai, Japan, 1992.
[26] D.J. Wheeler, in: Proc. Workshop on Chemical Reactivity on Oxide Fuel and Fission Product Release, Berkeley, UK, eds. K.A. Simpson and P. Wood (CEGB, London, 1987) p. 357.
[27] H.E. Kissinger, Anal. Chem. 11 (1957) 1702.
[28] H. Landspersky, M. Voboril, J. Inorg. Nucl. Chem. 29 (1966) 250.
[29] M.J. Bennett, J.B. Price, P. Wood, Nucl. Energy 27 (1988) 49.
[30] I.J. Hastings, J. Novak, in: Proc. of the US Nuclear Regulatory Commission, Workshop on Spent Fuel/Cladding Reaction During Dry Storage, Gaithersburg, USA, ed. D.W. Reisenweaver, Report NUREG/CP-0049, 1983, p. 26.
[31] I.J. Hastings, D.H. Rose, J.R. Kelm, D.A. Irvine, J. Am. Ceram. Soc. 69 (1986) C16.
[32] R.E. Einziger, R.V. Strain, Proc. Int. Workshop of Irradiated Fuel Storage: Operating Experience and Development Programs, held in Toronto, ON, 1984, p. 599.
[33] R.J. McEachern, J. Nucl. Mater. 245 (1997) 238.
[34] L.E. Thomas, R.E. Einziger, Mater. Charact. 28 (1992) 149.
[35] F.C. Tompkins, in: Treatise on Solid State Chemistry, Vol. 4, Reactivity of Solids, ed. N.B. Hannay (Plenum, New York, NY, 1976).
[36] V. Erukhimovitch, J. Baram, Phys. Rev. B51 (1995) 6221.
[37] P.A. Tempest, P.M. Tucker, J.W. Tyler, J. Nucl. Mater. 151 (1988) 251.
[38] T.K. Campbell, E.R. Gilbert, G.D. White, G.F. Piepel and, B.J. Wrona, Nucl. Technol. 85 (1989) 160.
[39] J.W. Choi, R.J. McEachern, P. Taylor, D.D. Wood, J. Nucl. Mater. 230 (1996) 250.